

# Band-edge BCS–BEC crossover in a two-band superconductor: physical properties and detection parameters

Andrea Guidini<sup>1</sup> and Andrea Perali<sup>2</sup>

<sup>1</sup>School of Science and Technology, Physics Division, University of Camerino, 62032 Camerino, Italy

<sup>2</sup>School of Pharmacy, Physics Unit, University of Camerino, 62032 Camerino, Italy

E-mail: [andrea.perali@unicam.it](mailto:andrea.perali@unicam.it)

Received 11 July 2014, revised 12 September 2014

Accepted for publication 30 September 2014

Published 31 October 2014

## Abstract

Superconductivity in iron-based magnesium diborides and other novel superconducting materials has a strong multi-band and multi-gap character. Recent experiments support the possibility for a BCS–BEC crossover induced by strong-coupling and proximity of the chemical potential to the edge of one of the bands. Here we study the simplest theoretical model which accounts for the BCS–BEC crossover in a two-band superconductor, considering tunable interactions and tunable energy separations between the bands. Mean-field results for condensate fraction, correlation length, and superconducting gap are reported in typical crossover diagrams to locate the boundaries of the BCS, crossover and BEC regimes. When the superconducting gap is of the order of the local chemical potential, superconductivity is in the crossover regime of the BCS–BEC crossover and the Fermi surface of the small band is smeared by the gap opening. In this situation, small and large Cooper pairs coexist in the total condensate, which is the optimal condition for high- $T_c$  superconductivity. The ratio between the gap and the Fermi energy in a given band results in the best detection parameter for experiments to locate the system in the BCS–BEC crossover. Using available experimental data, our analysis shows that iron-based superconductors have the partial condensate of the small Fermi surface in the crossover regime of the BCS–BEC crossover, supporting the recent ARPES findings.

Keywords: multi-band superconductivity, BCS–BEC crossover, multi-condensates

(Some figures may appear in colour only in the online journal)

## 1. Introduction

Multi-band and multi-gap superconductivity is emerging as a complex quantum coherent phenomenon with physical properties which are different from or cannot be found in single band conventional superconductors. The increased number of degrees of freedom of the multi-component superconducting wave-function allows for novel effects. Phase solitons [1] and massive or massless Leggett modes [2, 3] are possible benchmarks for multi-gap superconductivity, being associated with phase differences between the condensates in different electronic bands. Exotic vortex states [4], non-trivial interactions between the vortices [5] and hidden criticality [6] are also peculiar phenomena associated

with the multi-gap and multi-condensate nature of the superconducting state. In these systems, the total superconducting condensate results from the coherent mixture of partial condensates forming in each band, and the partial condensates can have very different properties, leading to interesting interference effects. Very recently, evidence of the BCS–BEC crossover and strong coupling superconductivity have been reported in the small Fermi surface pockets of multi-band superconductors. ARPES measurements in iron-chalcogenide superconductors have shown a superconducting gap to Fermi energy ratio of order unity in the shallow upper bands. The crossover regime has been detected by the collapse of the small Fermi surface pocket and by the electronic band dispersion becoming an inverted parabola in the

coherent state [7]. This phenomenology observed in iron-based superconductors is the same as the one predicted and observed in ultracold fermions [8, 9].

Moreover, in underdoped superconducting cuprates the bandwidth around the M points of the Brillouin zone is very narrow, of the same order of the gap and pseudogap. Evidences of broken Fermi surface and multi-band effects are also recently reported in YBCO superconducting cuprates due to charge ordering [10]. A sizable pseudogap, its continuous evolution across  $T_c$ , together with a short correlation length are evidence for strong pairing effects [11] and importance of the BCS–BEC crossover in the underdoped cuprate superconductors [12, 13].

Another motivation to study the BCS–BEC crossover in two-band superconductors comes from the superconducting properties of the iron-based superconductor  $\text{Ba}_{0.6}\text{K}_{0.4}\text{Fe}_2\text{As}_2$  ( $T_c = 37$  K). Two different s-wave gaps open in the different sheets of Fermi surface (FS): a large gap of  $\Delta_2 = 12$  meV on the small FS and a small gap  $\Delta_1 = 6$  meV in the large FS [14]. The ratio  $2\Delta_1/T_c = 3.7$  is very close to the BCS value of 3.5, indicating BCS-like weakly coupled pairs in the large FS, while  $2\Delta_2/T_c = 7.5$  is very large and typical of BEC-like strongly coupled pairs in the small FS. Hence, the total superconducting condensate in  $\text{BaKFeAs}$  is a coherent mixture of BCS-like and BEC-like partial condensates.

A two-gap superconductor with quite distinct gaps in the different bands is also  $\text{MgB}_2$ . In this material evidence for resonant and crossover phenomena due to proximity to a band edge have been reported [15].

Quantum confinement and shape resonance in stripe systems, proposed as a mechanism for  $T_c$  amplifications [16–18] with recent experimental confirmation in metallic stripes [19], are clearly in coexistence with BCS–BEC crossover, which can determine the best situation for high- $T_c$  superconductivity. Indeed, multi-band BCS–BEC crossover can determine the optimal condition to allow the screening of superconducting fluctuations. This screening effect is expected to be active in a two-band superconductor, as shown by means of a Ginzburg–Landau approach in [12].

Quite generally, different families of iron-based superconductors show new small Fermi surfaces at optimum doping where  $T_c$  is the highest, appearing when the chemical potential is near a band edge, close to the bottom (if electron-like) or top (if hole-like) of the energy bands [20]. In this situation, experiments show no evidence for nesting topology and the mechanism for high- $T_c$  can be associated with the shape resonance scenario [21]. In figures 1(a) and (b) of [21] the Fermi surfaces topology for different superconducting iron-based materials have been schematized, showing that in all cases large Fermi surfaces coexist with small Fermi surface pockets, supporting the (at least) two-band model for superconductivity as the minimal model to capture the band-edge physics and corresponding novel multi-band BCS–BEC crossover phenomena.

In 2D electron gases numerical evidence based on Bogoliubov–de Gennes equations for the BCS–BEC crossover in surface superconductivity have been found. In such systems the crossover phenomenon can be explored by

controlling the gate voltage of the surface superconductivity. A gap to Fermi energy ratio larger than one signals the realization of the BEC regime in one of the bands of  $\text{SrTiO}_3$ , whereas the other bands are in the BCS regime, having a gap to Fermi energy ratio smaller than one [22].

Finally, in ultracold cigar-shaped Fermi gases the quantum confinement induces the formation of a series of single-particle subbands. As theoretically predicted in [23], in the superfluid state of these systems the total condensate is a coherent mixture of subband condensates, each of which undergoes a BCS–BEC crossover when the edge of the corresponding subband approaches the chemical potential.

The BCS–BEC crossover in two-band ultracold fermions in the superfluid state has been studied at mean-field and Ginzburg–Landau level in [24]. The main results of [24] have been the understanding of the role of the interband (Josephson-like) coupling in driving the transition between a 0-phase and a  $\pi$ -phase of the two component order parameter, the undamped collective excitations and the finite temperature Ginzburg–Landau description of the two-band BCS–BEC crossover.

In this work we will focus on the BCS–BEC crossover which can be induced in one of the partial condensates when the chemical potential is close to the band edge of a two-band system. In our model system, one partial condensate is in the weak-coupling regime with extended Cooper pairs forming in the large Fermi surface, while the second partial condensate has tunable properties, and the pairing in the small Fermi surface can be varied from the weak- to the strong-coupling regime, allowing for the BCS–BEC crossover to be induced in the band associated with the small Fermi surface. We will explore at mean-field level and at zero temperature, in a three dimensional continuum, the phase space of the interaction parameters in order to detect the boundaries between the different BCS, crossover and BEC regimes, locating in the boundary diagrams the available experimental data of multi-gap superconductors.

The physical description of the zero temperature BCS–BEC crossover [25, 26] is based on two physical quantities: the condensate fraction [27] and the average size of the Cooper pairs [28]. The condensate fraction quantifies the fraction of fermions participating in the condensation into the superconducting state. In the BCS regime the condensate fraction is exponentially small and a very small density of fermions forms the condensate wave-function; in the BEC regime the condensate fraction approaches unity, i.e. the attraction is so strong that all the fermions form local molecular pairs with bosonic character. In terms of the average pair size  $\xi_{\text{pair}}$  the physics is well known, as the parameter  $k_F \xi_{\text{pair}}$  was the first parameter used in the pioneering work on the BCS–BEC crossover [28]. The BCS regime is characterized by  $k_F \xi_{\text{pair}} \gg 1$ , while in the BEC regime point-like pairs lead to  $k_F \xi_{\text{pair}} < 1$ . This characterization of the BCS–BEC crossover ends up being very clear from a theoretical and phenomenological point of view, but unfortunately both the condensate fraction and the average size of the pairs are not easy to measure. Hence, in this work we provide a way to link

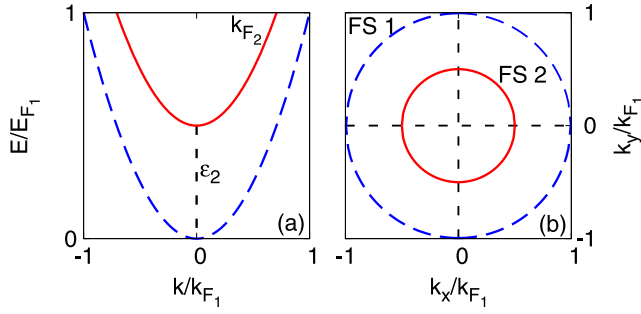


**Figure 1.** Band dispersions (panel (a)) and  $k_z = 0$  projection of the Fermi surfaces (panel (b)). The energy and the wave-vectors are measured in units of  $E_{F1}$  and  $k_{F1}$ , respectively.  $\epsilon_2$  is the band offset of the upper band and it is measured in units of  $E_{F1}$ .

the BCS–BEC crossover given in terms of the condensate fraction  $\alpha$  and  $k_F \xi_{\text{pair}}$  to the ratio between the superconducting pairing gap at  $T = 0$  to the Fermi energy of the non-interacting system. This ratio is measurable in experiments by ARPES, tunnelling (STM) or specific heat measurements and can then provide a very useful parameter to detect the BCS–BEC crossover in complex multi-gap superconductors, as in the case of iron-pnictides,  $\text{MgB}_2$  or cuprates.

The paper is organized as follows. In section 2 we will discuss the model system, the mean-field equations that describe it and the relevant physical quantities used to detect the boundaries of the BCS–BEC crossover. In section 3 we will present our results for the one-band system as a reference, and then we will discuss the results for the two-band system in connection with available experimental data. Section 4 presents our concluding remarks.

## 2. Model and methods

A two-band system of interacting fermions in three dimensions and at zero temperature is considered. The two electronic bands have a parabolic dispersion  $\xi_i(\mathbf{k})$  given by:

$$\xi_i(\mathbf{k}) = \frac{\mathbf{k}^2}{2m} - \mu + \epsilon_i, \quad (1)$$

where  $\mathbf{k}$  is the wave-vector,  $m$  the effective mass which is taken equal in the two-bands,  $\mu$  the chemical potential and  $\epsilon_i$  the energy of the bottom of the bands. The index  $i = 1, 2$  labels the bands:  $i = 1$  denotes the lower band and  $i = 2$  denotes the upper band. We set  $\epsilon_1 = 0$ , while  $\epsilon_2 \geq 0$  is tunable. The Fermi energies  $E_{F_i}$  are defined in the non-interacting case as  $E_{F_i} = \mu - \epsilon_i$ . We also set  $\hbar = 1$  throughout this article.

In figure 1 the band dispersions and the Fermi surfaces are reported. The effective pairing interaction between fermions is approximated by a separable potential  $V_{ij}(\mathbf{k}, \mathbf{k}')$  with an energy cutoff  $\omega_0$  and it is given by:

$$V_{ij}(\mathbf{k}, \mathbf{k}') = -V_{ij}^0 \Theta(\omega_0 - |\xi_i(\mathbf{k})|) \Theta(\omega_0 - |\xi_j(\mathbf{k}')|), \quad (2)$$

where  $V_{ij}^0$  is the (positive) strength of the potential and  $i, j$  label the bands. In the following we will set  $V_{ij}^0 = V_{ji}^0$ .  $V_{11}^0$  and  $V_{22}^0$

are the strength of the intraband pairing interactions (Cooper pairs are created and destroyed in the same band).  $V_{12}^0 = V_{21}^0$  are the strength of the Josephson-like interband pairing interactions (Cooper pairs are created in one band and destroyed in the other band, and vice versa). Here we consider the same energy cutoff  $\omega_0$  of the interaction for intraband and interband pairing terms. Note that in this work we neglect interband pairing terms corresponding to Cooper pairs forming from fermions associated to different bands. Moreover, when the chemical potential relative to the bottom of the bands becomes negative, the replacement  $\mu - \epsilon_i \rightarrow 0$  will be done in both of the step functions of equation (2) to obtain the correct BEC limit given by the corresponding two-body problem in the vacuum. Indeed, when  $\mu - \epsilon_i$  is negative the Fermi surface of the band ( $i$ ) is destroyed and the interaction becomes contact-like, with a cutoff in  $\mathbf{k}$  ( $k_0 = \sqrt{2m\omega_0}$ ) which ensures the convergence of the mean-field equations.

The superconducting ground state of our system is studied in this article at a mean-field level of approximation. We use mean-field equations at zero temperature based on the two-band extension of the mean-field BCS theory [29]. The BCS equations for the two superconducting gaps are coupled with the equation for the total density of the system, as the renormalization of the chemical potential is a key feature in the BCS–BEC crossover [13, 28].

The equations for the gaps  $\Delta_1(\mathbf{k})$  and  $\Delta_2(\mathbf{k})$  read:

$$\Delta_1(\mathbf{k}) = -\frac{1}{\Omega} \sum_{\mathbf{k}'} \left[ V_{11}(\mathbf{k}, \mathbf{k}') \frac{\Delta_1(\mathbf{k}')}{2\sqrt{\xi_1(\mathbf{k}')^2 + \Delta_1(\mathbf{k}')^2}} + V_{12}(\mathbf{k}, \mathbf{k}') \frac{\Delta_2(\mathbf{k}')}{2\sqrt{\xi_2(\mathbf{k}')^2 + \Delta_2(\mathbf{k}')^2}} \right], \quad (3)$$

$$\Delta_2(\mathbf{k}) = -\frac{1}{\Omega} \sum_{\mathbf{k}'} \left[ V_{21}(\mathbf{k}, \mathbf{k}') \frac{\Delta_1(\mathbf{k}')}{2\sqrt{\xi_1(\mathbf{k}')^2 + \Delta_1(\mathbf{k}')^2}} + V_{22}(\mathbf{k}, \mathbf{k}') \frac{\Delta_2(\mathbf{k}')}{2\sqrt{\xi_2(\mathbf{k}')^2 + \Delta_2(\mathbf{k}')^2}} \right], \quad (4)$$

being  $\Omega$  the volume occupied by the system, and with the gaps having the same cutoff of the separable interaction:

$$\Delta_i(\mathbf{k}) = \Delta_i \Theta(\omega_0 - |\xi_i(\mathbf{k})|). \quad (5)$$

Note that the step function of equation (5) also undergoes the same replacement discussed above for the interaction potential in the case  $\mu - \epsilon_i < 0$ .

In this work, the total density of the two-band system is fixed and it is given by the sum of the densities in the two-bands,  $n_{\text{tot}} = n_1 + n_2$ . The fermionic density  $n_i$  in the band ( $i$ ) at  $T = 0$  is defined as:

$$n_i = \frac{2}{\Omega} \sum_{\mathbf{k}} v_i(\mathbf{k})^2, \quad (6)$$

where  $v_i(\mathbf{k})$  is the BCS weight of the occupied states. The

BCS weights  $v_i(\mathbf{k})$  and  $u_i(\mathbf{k})$  are:

$$v_i(\mathbf{k})^2 = \frac{1}{2} \left[ 1 - \frac{\xi_i(\mathbf{k})}{\sqrt{\xi_i(\mathbf{k})^2 + \Delta_i(\mathbf{k})^2}} \right], \quad (7)$$

$$u_i(\mathbf{k})^2 = 1 - v_i(\mathbf{k})^2. \quad (8)$$

The boundaries between the different BCS, crossover and BEC regimes of the two-band BCS–BEC crossover are here determined by analyzing three fundamental physical quantities of the superconducting ground state wave function: the condensate fraction, the correlation length of the Cooper pairs and the superconducting gap, using physical insights from the BCS–BEC crossover in ultracold fermionic atoms close to a Fano–Feshbach resonance [27, 28]. The condensate fraction  $\alpha_i$ , which is the ratio between the number of fermions of the band ( $i$ ) forming the Cooper pairs of the condensate and the total number of fermionic particles in the same band, strictly related to the off-diagonal long-range order, is defined as:

$$\alpha_i = \frac{\sum_{\mathbf{k}} (u_i(\mathbf{k})v_i(\mathbf{k}))^2}{\sum_{\mathbf{k}} v_i(\mathbf{k})^2}, \quad (9)$$

while the pair correlation length  $\xi_{\text{pair},i}$ , which represents the average size of the Cooper pairs, is given by:

$$\xi_{\text{pair},i} = \left[ \frac{\sum_{\mathbf{k}} |\nabla_{\mathbf{k}} (u_i(\mathbf{k})v_i(\mathbf{k}))|^2}{\sum_{\mathbf{k}} (u_i(\mathbf{k})v_i(\mathbf{k}))^2} \right]^{\frac{1}{2}}. \quad (10)$$

In equation (10) the step function of equation (5) is replaced by a smooth function in order to obtain finite partial derivatives.

We solve numerically the three by three system of equations (3), (4) and (6). We perform numerical calculations using a Fortran95 program in which we use the Gauss–Legendre method to evaluate the integrals over the energy variable  $\epsilon = k^2/(2m)$  and the symmetric rank-one method to solve systems of equations. Once the values of the gaps and of the chemical potential are obtained, we calculate numerically the condensate fraction and the pair correlation length given in equations (9) and (10) respectively.

For the one-band system we use as units  $k_F$  for wave-vectors, where  $k_F = (6\pi^2 n)^{1/3}$  and  $n$  is the density of a free Fermi gas. We use then the Fermi energy scale  $E_F = \frac{k_F^2}{2m}$  to normalize the energies. The dimensionless coupling  $\lambda$  is defined as  $\lambda = N(E_F)V^0$  where  $N(E_F)$  is the density of states at the Fermi level (note that in the one-band case we dropped the indices used in section 2 to label the bands).

For the two-band system, as we are mostly interested in the properties of the upper band (label 2), we use the units of band 2 and energies are measured in units of  $E_{F_2} = E_{F_1}(1 - \frac{\epsilon_2}{E_{F_1}})$ , where  $E_{F_1}$  is the Fermi energy of the lower band. The dimensionless coupling in the upper band is  $\lambda_{22}^{\text{eff}} = \lambda_{22} \sqrt{1 - \frac{\epsilon_2}{E_{F_1}}}$ , with  $\lambda_{22} = N(E_{F_1})V_{22}^0$ . The interband (Josephson-like) coupling parameters are defined as  $\lambda_{12} = N(E_{F_1})V_{12}^0$  and  $\lambda_{21} = N(E_{F_1})V_{21}^0$ . With this definition,

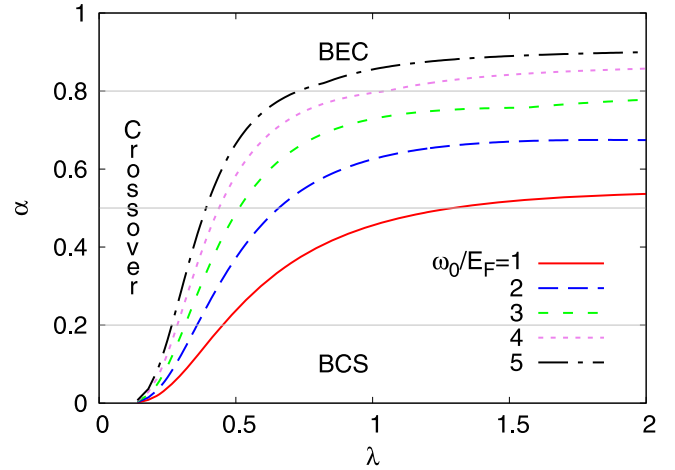


**Figure 2.** Condensate fraction  $\alpha$  in the one-band case as a function of coupling  $\lambda$  for different energy cutoffs of the interaction  $\omega_0$  normalized to the Fermi energy. Thin solid lines (grey color online) correspond to  $\alpha = 0.2, 0.5, 0.8$  from bottom to top.

we obtain  $\lambda_{12} = \lambda_{21}$ , being  $V_{12}^0 = V_{21}^0$ . The total density of fermions in our system is then  $n_{\text{tot}} = n_1 \left[ 1 + \left( 1 - \frac{\epsilon_2}{E_{F_1}} \right)^{3/2} \right]$ .

### 3. Results

The first step in our analysis is to study the properties of the superconducting ground state with only one band and the separable interaction considered in this work. It turns out that a full characterization of the BCS–BEC crossover for this fermionic system is lacking in the literature even in the one-band case. As described in the previous section, the line boundaries between the BCS, crossover and BEC regimes are determined through the calculation of the condensate fraction given in equation (9), of the correlation length of the Cooper pairs given in equation (10) and of the superconducting gap obtained by reducing equations (3)–(6) to the standard one-band case. The aim is to verify that the crossover boundary lines obtained with condensate fraction, correlation length, and superconducting gap are compatible with each other.

In figure 2 the condensate fraction  $\alpha$  is reported as a function of the coupling  $\lambda$  for different energy cutoffs of the pairing interaction. This quantity will guide us to the exploration of the crossover boundary diagrams and to establish the boundaries for the gap and the pair correlation length. Thin horizontal lines (grey color online) represent our choice of the boundaries between the different pairing regimes: for  $\alpha < 0.2$  the superconducting state is in the weak-coupling BCS regime; for  $0.2 < \alpha < 0.8$  the system is in the crossover regime; for  $\alpha > 0.8$  the system is in the strong-coupling BEC regime ( $\alpha = 1$  corresponds to all fermions paired in a bosonic state). The line  $\alpha = 0.5$  indicates the centre of the BCS–BEC crossover, corresponding to having 50% of fermions in the condensed state. Note that for  $\lambda < 0.25$  the condensate fraction, being directly proportional to the gap, is exponentially suppressed, and the number of

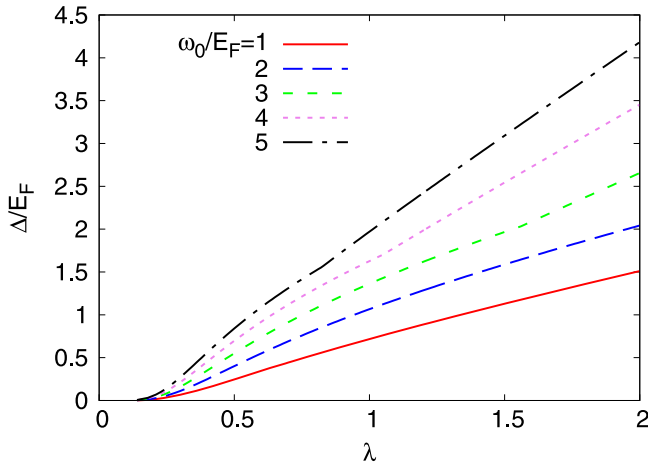


**Figure 3.** Superconducting gap  $\Delta$  in the one-band case as a function of the coupling  $\lambda$  for different energy cutoffs of the interaction  $\omega_0$  normalized to the Fermi energy.

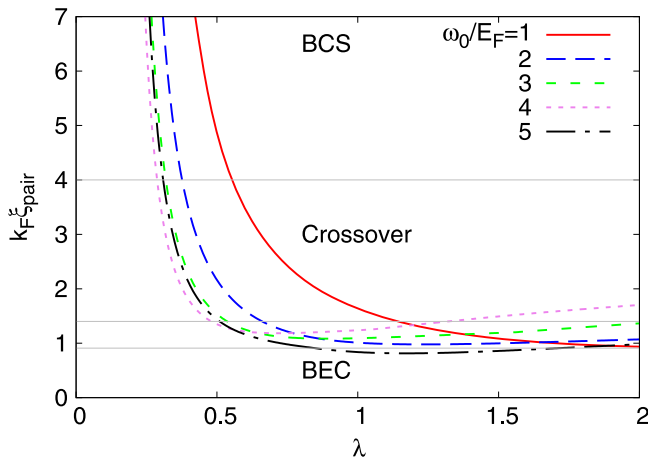


**Figure 4.** Correlation length (average size of the Cooper pairs)  $k_F \xi_{\text{pair}}$  in the one-band case as a function of the coupling  $\lambda$  for different energy cutoffs of the interaction  $\omega_0$  normalized to the Fermi energy. Thin solid lines (grey color online) correspond to  $k_F \xi_{\text{pair}} = 0.91, 1.4, 4.0$  from bottom to top.

fermions entering in the condensate becomes extremely small. The proportionality between the gap and the condensate fraction in the BCS regime has also been obtained for ultracold fermions at mean-field level [27]. Note in figure 2 that when the pairing is increased the condensate fraction saturates to values that increase for increasing energy cutoff: as a consequence, while the crossover regime can be easily approached for different cutoff values, the BEC regime requires strong pairing and a large energy cutoff to localize the Cooper pairs in space (large wave vectors need to be coupled by the pairing interaction).

In figure 3 the superconducting gap in the one-band case is reported as a function of the coupling  $\lambda$  for different values of the energy cutoff  $\omega_0$ . The gap is exponentially suppressed for small values of the interaction  $\lambda < 0.25$  (the well known BCS weak-coupling limit  $\Delta = 2\omega_0 e^{-1/\lambda}$  has been recovered by our numerical calculations) and it increases for larger value of the interaction when the BEC limit is approached. The gap

gets larger and larger when the energy cutoff  $\omega_0$  is increased. In the plot for the coupling dependence of the gap for different energy cutoffs, it is not possible to find a single value of the gap which is in correspondence to the boundary values of the condensate fraction as shown later in this section.

In figure 4 the correlation length of the Cooper pairs is presented as a function of the coupling  $\lambda$  for different values of the energy cutoff  $\omega_0$ . Thin grey lines represent the boundaries that we have found to match the crossover boundary diagram for  $k_F \xi_{\text{pair}}$  with that of  $\alpha$  (see panel (c) of figure 5). We obtain a satisfactory matching using  $k_F \xi_{\text{pair}} = 4.0$  for the BCS boundary line,  $k_F \xi_{\text{pair}} = 1.4$  for the center of the crossover line and  $k_F \xi_{\text{pair}} = 0.91$  for the BEC line. The calculation of  $k_F \xi_{\text{pair}}$  requires the introduction of a smearing procedure of the step function of equation (5) in order to perform the numerical derivatives of equation (10). In figure 4 the line corresponding to  $\omega_0/E_F = 5$  has been obtained with a different smearing parameter ( $\omega_s/E_F = 4.0$ ) with respect to the other four curves ( $\omega_s/E_F = 0.1$ ), and it has been presented to show how the BEC limit is approached.

In the weak-coupling limit ( $\lambda \ll 1$ ) the correlation length diverges, while it decreases for larger values of the pairing interaction. We have verified that in the weak-coupling limit ( $\omega_0/E_F \lesssim 0.2$ ,  $\lambda \lesssim 0.2$ ) our results for the pair correlation length are in good agreement with that of [28]. Indeed we have found that our one-band system is in the BCS regime of pairing when the dimensionless parameter  $k_F \xi_{\text{pair}} > 4.0$  which is close to the value  $2\pi$  found in [28], corresponding to strongly overlapping Cooper pairs. More precisely, the boundary value for the BCS regime,  $k_F \xi_{\text{pair}} = 2\pi$  of [28], is obtained in our model system for  $\omega_0/E_F > 1$  and for a value of the condensate fraction  $\alpha = 0.13$ . Therefore, according to our choice of the boundary values,  $k_F \xi_{\text{pair}} = 2\pi$  describes a regime of pairing well inside the BCS regime. Moreover, as expected from the behaviour of the gap and of the condensate fraction, the pair correlation length also easily approaches the crossover regime, while it approaches the BEC regime only for strong coupling and large energy cutoffs.

Note that in the intermediate to strong-coupling regime ( $\lambda > 0.5$ ) the pair correlation length reported in figure 4 is characterized by an almost flat dependence on the coupling, with a non-monotonic behavior and a presence of a shallow minimum. This is indeed a counter-intuitive result because a monotonic decrease of  $\xi_{\text{pair}}$  toward the bound state radius approaching the BEC limit is expected. This complicated behavior is associated with the momentum cutoff of the pairing interaction and with the smoothing of the step functions in the numerical calculation of the correlation length. Indeed, the position of the minimum depends on the details of the interaction potential and of the smoothing function, as clear from figure 4. In the BEC limit, because of a finite cutoff in momentum  $k_0/k_F = \sqrt{\omega_0/E_F}$  in our model system, the correlation length approaches a finite value and the molecular pairs have a finite minimum size, as obtained from our numerical calculations. In the intermediate to strong-coupling regime the flat behavior of  $\xi_{\text{pair}}$  is associated with the flat coupling dependence of the ratio  $\Delta/|\mu|$ , which controls the

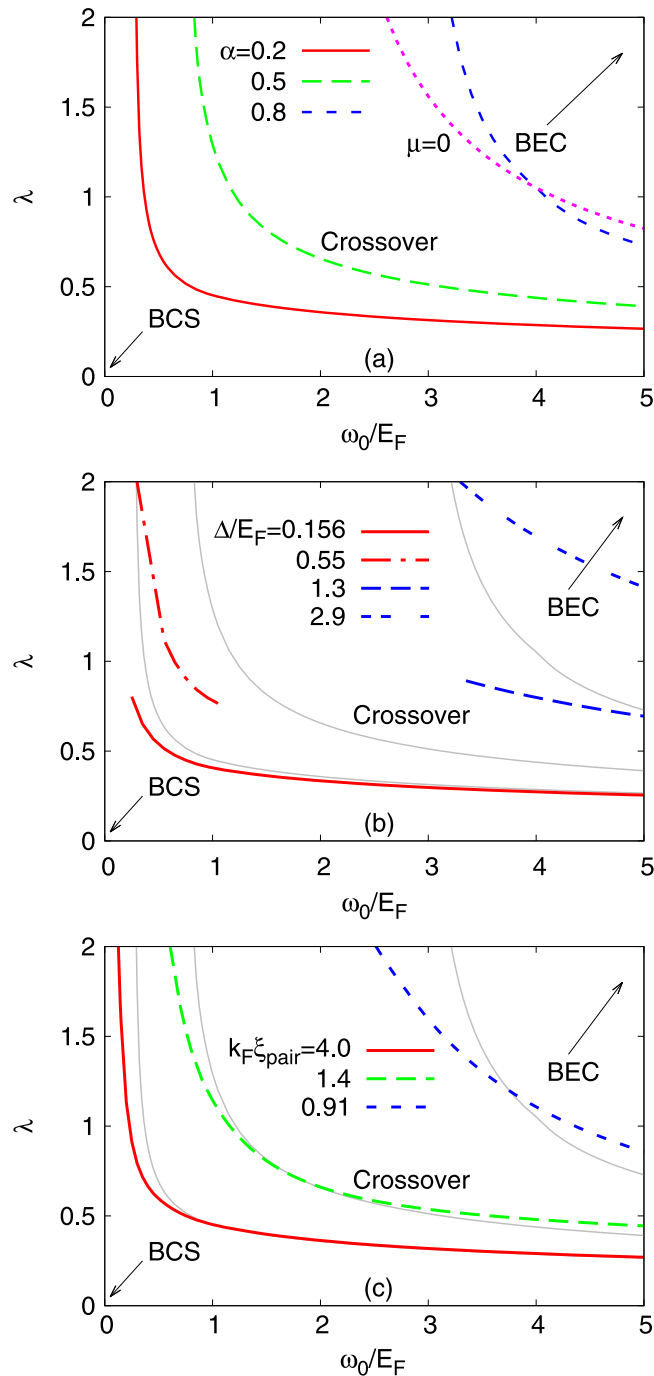


**Figure 5.** Crossover boundary diagrams for the BCS–BEC crossover in the one-band case in the coupling versus energy cutoff plane. Different lines indicate the crossover boundaries between the BCS, crossover and BEC regimes. The boundaries are obtained using the condensate fraction, the gap, and the correlation length. Panel (a): crossover boundary diagram for condensate fraction  $\alpha$  and curve for  $\mu = 0$ ; panel (b): crossover boundary diagram for condensate fraction (thin solid lines, grey color online) and gap  $\Delta$ ; panel (c): crossover boundary diagram for condensate fraction (same as in panel (b)) and pair correlation length  $\xi_{\text{pair}}$ .

coupling dependence of the correlation length approaching the BEC regime, which is  $k_F \xi_{\text{pair}} \approx (\Delta/|\mu|)^{2/3}$ , as shown in equation (37) of [30]. Hence, approaching the BEC limit, when the pairing interaction is different from a pure contact

potential, is a complicated process and the correlation length is a quite involved physical quantity to follow in this part of the BCS–BEC crossover. However, this behaviour of the correlation length does not affect the boundary diagrams that will be presented in the next section, because to obtain such diagrams we considered only the region where the correlation length is a decreasing function of the coupling, and is weakly dependent on the details of the interaction potential and of the smoothing function.

### 3.1. Crossover boundary diagrams

We present here the crossover boundary diagrams for the one-band system and for the two-band system. We consider the line boundary between the BCS and the crossover regime, the line corresponding to the center of the crossover, and the boundary line between the crossover and the BEC regime. In both one- and two-band systems, the constant values of the condensate fraction determine the crossover boundary lines. Along these boundaries we will extract the corresponding values of the pair correlation length and of the superconducting gap, which will be used as our detection parameters to locate the novel superconducting materials, i.e. the iron-pnictides, in the BCS–BEC crossover phase boundary diagrams. In the case of the two-band system, our analysis of the BCS–BEC crossover will be focused on the upper band for chemical potentials close to the bottom of the upper band.

**3.1.1. One-band system.** Panels (a), (b) and (c) of figure 5 present the crossover boundary diagrams for the condensate fraction (panel (a)), gap (panel (b)) and pair correlation length (panel (c)) for the one-band system.

In panel (a) of figure 5 the crossover boundary diagram for the condensate fraction is presented together with the line that marks the change of sign of the chemical potential. In order to approach the BEC regime for the condensate fraction, it is necessary that the chemical potential becomes negative. This can be seen by comparing the boundary crossover lines for  $\mu = 0$  and  $\alpha = 0.8$ . This is already an important result. From the physics of the BCS–BEC crossover in ultracold fermions, we know that  $\mu = 0$  corresponds to entering the BEC regime [9]. Therefore we confirm that when more than 80% of fermions are paired and condensed, the system has entered the BEC regime.

Concerning the chemical potential we have found that in the BEC limit ( $\lambda \gg 1$  and  $\omega_0/E_F \gg 1$ ) the chemical potential  $\mu$  approaches half of the binding energy of two particles which interact in the vacuum through the potential defined in equation (2). This result confirms the correct treatment of the BEC limit that we have discussed in the previous section. The equation that defines the (negative) binding energy  $\epsilon_0$  of the two-body problem in the vacuum for a three dimensional system and the attractive interaction

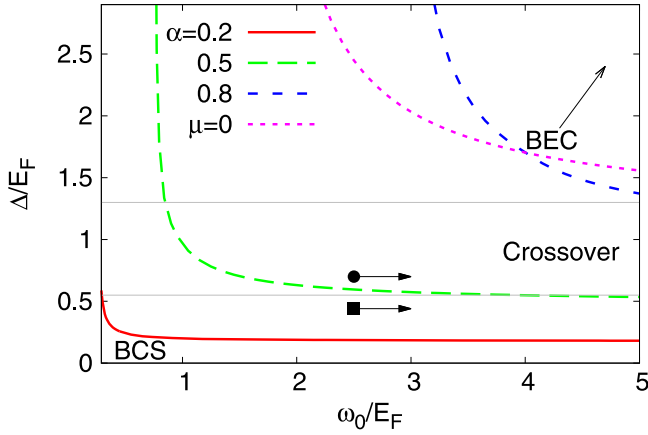


**Figure 6.** Crossover boundary diagram in the one-band case for the gap  $\Delta/E_F$  as a function of the cutoff frequency  $\omega_0/E_F$ , which correspond to the condensate fractions  $\alpha = 0.2, 0.5$  and  $0.8$  and  $\mu = 0$ . Thin horizontal lines (grey color online) represent the values  $\Delta/E_F = 0.55$  and  $1.3$  between which we have found that the system is in the crossover regime of pairing for every value of the coupling  $\lambda$  and of the cutoff energy  $\omega_0$  considered in this work. The points located at  $\Delta/E_F = 0.44$  and  $0.70$  correspond to two values of the pairing gap for ultracold fermions in the crossover regime reported in [31].

of equation (2) is:

$$\frac{1}{\lambda} = \int_0^{\omega_0} d\epsilon \frac{\sqrt{\epsilon}}{2\epsilon + |\epsilon_0|}, \quad (11)$$

that has the implicit solution for  $\epsilon_0$ :

$$\frac{1}{\lambda} = \sqrt{\omega_0} - \sqrt{\frac{|\epsilon_0|}{2}} \arctan \sqrt{\frac{2\omega_0}{|\epsilon_0|}}, \quad (12)$$

where energy variables of equations (11) and (12) have been normalized to an energy scale  $E_F$ . In our many body system, we have verified that  $\mu \rightarrow -|\epsilon_0|/2$  for sufficiently large values of the coupling  $\lambda$  and of the energy cutoff  $\omega_0$ . For instance this BEC limit is obtained with our set of equations for  $\omega_0/E_F \sim 6$  and  $\lambda \sim 3$ . We have also found that there exists a critical value of the coupling  $\lambda_c = 1/\sqrt{\omega_0}$  (in units of a generic energy scale  $E_F$ ) below which no two-body bound state is allowed: the existence of a coupling threshold for two-body bound state is a generic feature in 3D systems.

In panel (b) of figure 5 the guiding crossover boundary diagram for the condensate fraction (thin grey lines) is presented together with the gap crossover boundary diagram. We choose the boundaries for the gap in order to match the condensate fraction crossover boundary lines at  $\lambda = 2$  and at  $\omega_0/E_F = 5$ . We then choose  $\Delta/E_F = 0.156$  and  $\Delta/E_F = 1.3$  as lower bounds at  $\omega_0/E_F = 5$  for the BCS and the BEC lines respectively, and  $\Delta/E_F = 0.55$  and  $2.9$  as upper bounds for the gap at  $\lambda = 2$ . Note that  $\Delta/E_F = 0.156$  is the value of the gap corresponding to  $k_F \xi_{\text{pair}} = 4.8$ .

In panel (c) of figure 5 the guiding crossover boundary diagram for the condensate fraction is presented together with the correlation length crossover boundary diagram. The boundaries for the BCS, center of the crossover and BEC

regimes are  $k_F \xi_{\text{pair}} = 4.0, 1.4$  and  $0.91$  respectively. One can see that the BCS and center of the crossover boundary lines for the pair correlation length and for the condensate fraction are in good agreement for all the values of energy cutoff. The BEC line has the same qualitative behaviour of that for  $\alpha = 0.8$  and it is in very good agreement with the  $\mu = 0$  curve of panel (a).

To obtain the boundary lines for the correlation length we use a different smearing parameter per each boundary line: we choose  $\omega_s/E_F = 0.1, 0.8$  and  $4$  for the BCS, center of the crossover and BEC lines respectively.

To conclude the analysis of the BCS–BEC crossover in the one-band system we show in figure 6 the crossover boundary diagram that presents the values of the gap to which correspond condensate fractions  $\alpha = 0.2, 0.5$  and  $0.8$ , and  $\mu = 0$ . The remarkable result that emerges from figure 6 is that values of the gap between  $\Delta/E_F = 0.55$  and  $1.3$  permit us to locate the system in the crossover regime of the BCS–BEC crossover for all the values of the energy cutoff  $\omega_0/E_F = (0,5)$  and of the coupling  $\lambda = (0,2)$  considered in this work. In figure 6 we report for comparison the available experimental values of the ratio  $\Delta/E_F$  reported in [31] for ultracold fermionic atoms. The  $\Delta/E_F$  data points are reported in figure 6 with one arrow to indicate that the results of the contact potential can be obtained by using a separable attractive interaction only in the limit of large  $\omega_0/E_F$  and small coupling  $\lambda$ .

Using the crossover boundary diagram of figure 6 one can identify immediately the values of the gap that permit us to locate the superconducting system in the BCS, crossover or BEC regimes. Independently from the details of the pairing interaction, our results show that when  $0.55 < \Delta/E_F < 1.3$  the one-band system is in the center of the BCS–BEC crossover and  $\Delta/E_F$  can be considered as a robust detection parameter to characterize the regime of pairing.

**3.1.2. Two-band system.** Figure 7 presents the crossover boundary diagrams for the partial condensate fraction in the upper band  $\alpha_2$  and for the change of sign of the chemical potential with respect to the bottom energy of the upper band  $\mu - \epsilon_2 = 0$ . We consider the coupling  $\lambda_{22}^{\text{eff}}$  vs energy cutoff  $\omega_0/E_{F_2}$  plane for parameters  $\lambda_{11} = 0.15, \epsilon_2 = 0.5$ , for values of  $\lambda_{12} = \lambda_{21} = 0.05, 0.15, 0.25$  (panels (a), (b) and (c) respectively). With the present choice of parameters the Cooper pairing in band 1 is in the weak coupling regime ( $0.01 < \Delta_1/E_{F_1} < 0.5$ ), the interband pairing is progressively increased and the chemical potential is close to the upper band bottom, being  $\mu - \epsilon_2$  on the same energy scale of the gap in band 2 and of the energy cutoff of the interaction. In figure 7 the guiding lines for  $\alpha = 0.2, 0.5$  and  $\mu = 0$  (thin grey lines) of the one-band system (from panel (a) of figure 5) are presented together with the crossover boundary diagrams for the two-band system for  $\alpha_2 = 0.2, 0.5$  and  $\mu - \epsilon_2 = 0$ . In panel (a) of figure 7 corresponding to  $\lambda_{12} = \lambda_{21} = 0.05$ , the BCS boundary line is almost not affected by the presence of the lower band whereas the center of the crossover boundary line is slightly retarded for  $\omega_0/E_{F_2} \lesssim 1.5$ . In panel (b) and (c) of

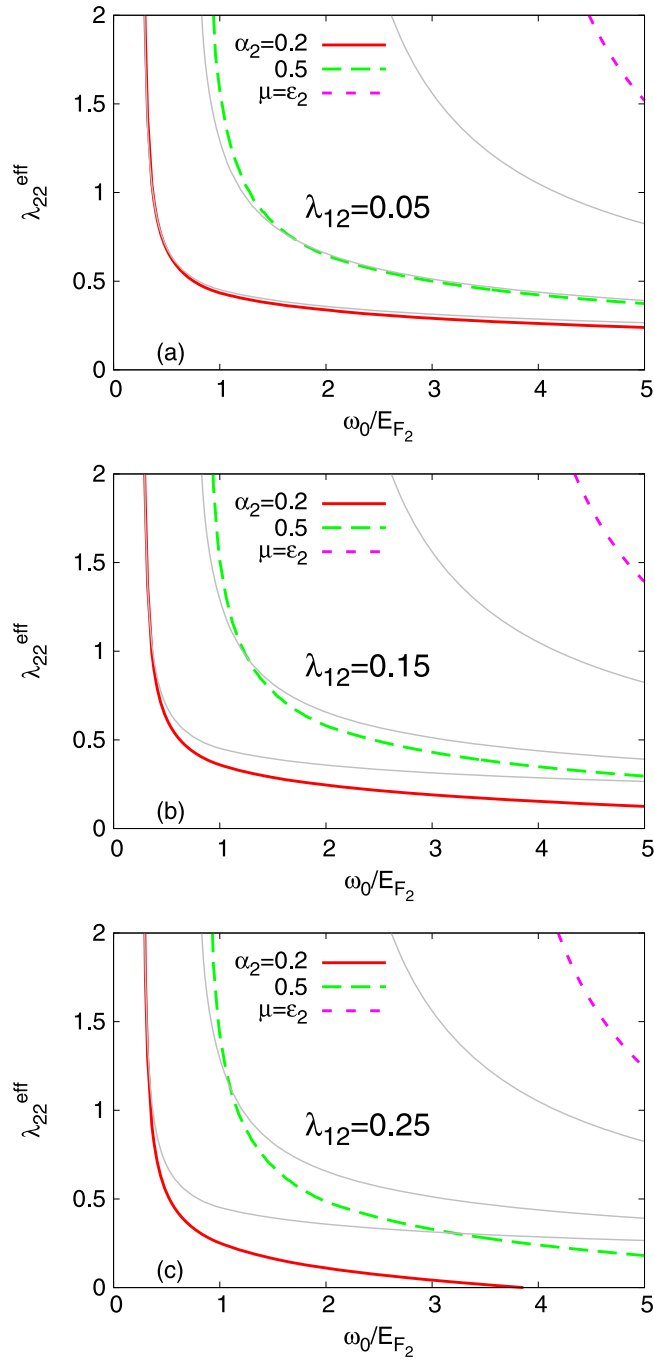


**Figure 7.** Crossover boundary diagrams for the BCS–BEC crossover in the two-band case in the coupling vs energy cutoff plane for  $\epsilon_2/E_{F_1} = 0.5$ ,  $\lambda_{11} = 0.15$ . The boundary lines for  $\alpha_2 = 0.2, 0.5$  and  $\mu = \epsilon_2$  for the two-band system are presented together with the lines for  $\alpha = 0.2, 0.5$  and  $\mu = 0$  for the one-band system (thin grey lines) as references. Different interband (Josephson-like) couplings are reported:  $\lambda_{12} = 0.05$  panel (a);  $\lambda_{12} = 0.15$  panel (b);  $\lambda_{12} = 0.25$  panel (c).

figure 7 the BCS boundary line is not affected with respect to that of the one-band system for  $\omega_0/E_{F_2} \lesssim 0.5$  and is progressively anticipated with increasing  $\lambda_{12}$  for  $\omega_0/E_{F_2} \gtrsim 0.5$ . The center of the crossover boundary line is slightly retarded and not affected by variation of  $\lambda_{12}$  for  $\omega_0/E_{F_2} \lesssim 1.1$

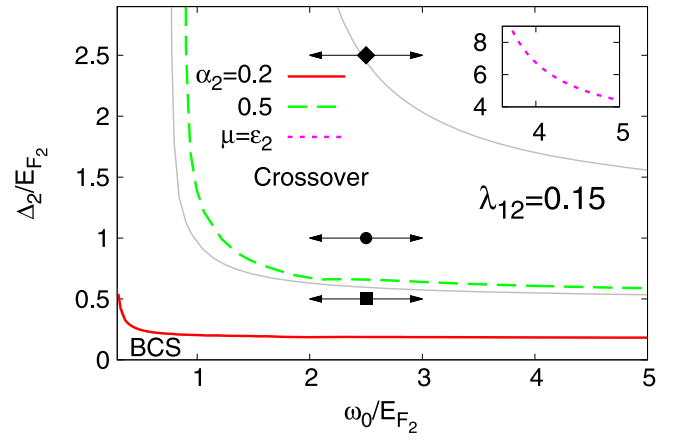


**Figure 8.** Crossover boundary diagram for the gap  $\Delta_2/E_{F_2}$  as a function of the cutoff frequency  $\omega_0/E_{F_2}$  to which correspond condensate fractions  $\alpha_2 = 0.2, 0.5$  and chemical potential  $\mu = \epsilon_2$  in the two-band system with  $\epsilon_2 = 0.5$ ,  $\lambda_{11} = \lambda_{12} = \lambda_{21} = 0.15$ . The lines for the one-band system (thin grey lines) for the gap  $\Delta/E_F$  to which correspond condensate fractions  $\alpha = 0.2, 0.5$  and chemical potential  $\mu = 0$  are also reported for reference. Inset: value of the  $\Delta_2/E_{F_2}$  when  $\mu = \epsilon_2$ . The points  $\Delta_2/E_{F_2} = 0.5, 1.0$  and  $2.5$  correspond respectively to the experimental values reported in [7], [32] and [33].

and is progressively anticipated for increasing  $\lambda_{12}$  for  $\omega_0/E_{F_2} \gtrsim 1.1$ . For all chosen values of  $\lambda_{12}$  the value  $\alpha_2 = 0.8$  needed to enter the BEC regime is not reached in the two-band system. Moreover in the two-band system the curve for the change of sign of the chemical potential with respect to the bottom of the upper band ( $\mu - \epsilon_2$ ) is significantly retarded with respect to that of the one-band system. This is because the presence of the lower band (having a gap smaller than the gap in the upper band) locks the chemical potential and does not permit it to decrease as fast as in the one-band system. As a consequence, the boundary line  $\mu = \epsilon_2$  is reached only for very large values of  $\omega_0/E_{F_2}$  and  $\lambda_{22}^{\text{eff}}$ . The line  $\mu - \epsilon_2 = 0$  is progressively anticipated for increasing values of  $\lambda_{12}$ .

Note that the line for  $\alpha_2 = 0.2$  in panel (c) vanishes at  $\omega_0/E_{F_2} \sim 4$  meaning that the system is already out of the BCS regime; it also features zero intraband coupling in band 2 because of the sizeable interband coupling  $\lambda_{12}$ .

In figure 8 the boundary crossover diagrams reporting the values of the gap  $\Delta_2/E_{F_2}$  that give  $\alpha_2 = 0.2, 0.5$  and  $\mu - \epsilon_2 = 0$  (inset) are presented for the two-band system using the same parameters in panel (b) of figure 7, together with the lines for the one-band system presented in figure 6 (we present in figure 8 the lines for  $\alpha = 0.2, 0.5$  and  $\mu = 0$  for the one-band system). This is the central result of our work for the two-band system.

One can see in figure 8 that the BCS gap line of the two-band system corresponding to a partial condensate fraction in band 2 of  $\alpha_2 = 0.2$  perfectly overlaps the line of the one-band system, whereas the center of the crossover line is slightly shifted up. The BEC line  $\alpha_2 = 0.8$ , as we said above, is not reachable in the two-band system, whereas the line for  $\mu = \epsilon_2$



is out of the chosen range ( $\Delta_2/E_{F_2} \sim 6$  presented in the inset). In figure 8 we report for comparison the available experimental values of the ratio  $\Delta_2/E_{F_2}$  for iron-based superconductors measured by ARPES. In the case of  $\text{FeSe}_x\text{Te}_{1-x}$  the gap to  $E_F$  ratio in the small upper band is  $\Delta_2/E_{F_2} \approx 0.5$  for  $x = 0.35$  [7] while for  $x = 0.40$  is  $\Delta_2/E_{F_2} \approx 1.0$  [32]. On the other hand very recent ARPES results give  $\Delta_2/E_{F_2} \approx 2.5$  for  $\text{LiFe}_{1-x}\text{Co}_x\text{As}$  ( $x = 0$ ) and a negative chemical potential with a finite gap for the same compound with 1 % and 3 % Co-doping [33]. The  $\Delta_2/E_{F_2}$  data points are reported in figure 8 with two arrows to indicate that the characteristic energy scale of the pairing interaction is not known, but that it is of the order of or larger than the (local) Fermi energy of the upper band, having a pairing of electronic origin.

Therefore, the central result of our work is that: (i) the superconducting iron chalcogenides are in the middle of the crossover regime of the BCS–BEC crossover, while (ii) Co-doped iron-pnictide superconductors are close to the BEC regime, with the BEC character being more pronounced for increasing Co-doping.

Our conclusion is that the two-band system with moderate intraband coupling for  $0.55 < \Delta_2/E_{F_2} < 4$  is in the crossover regime of the BCS–BEC crossover for any choice of pairing  $\lambda_{22}^{\text{eff}}$  and cutoff frequency  $\omega_0/E_{F_2}$  considered in this paper. As a consequence the crossover region of the two-band system is wider than that of the one-band system. On the other hand, only extreme values of  $\Delta_2/E_{F_2} > 4$  and very large values of  $\omega_0/E_{F_2}$  (plausible for pairing glue having an electronic origin) will drive the system toward the BEC regime for the partial condensate in the upper band.

We will now discuss our results on the average size of the Cooper pairs in the two bands ( $k_{F_1}\xi_{\text{pair},1}$  and  $k_{F_2}\xi_{\text{pair},2}$ ). The ratio between the two gaps  $\Delta_2/\Delta_1$  will also be reported as being a quantity directly comparable with experiments. We consider here two cases in the crossover regime in figure 8:

(i) for  $\Delta_2/E_{F_2} = 1$  and  $\omega_0/E_{F_2} = 2.5$  we obtain  $k_{F_1}\xi_{\text{pair},1} = 8.4$  and  $k_{F_2}\xi_{\text{pair},2} = 1.2$  with a ratio  $\Delta_2/\Delta_1 = 4$ . In this situation we have extended overlapping Cooper pairs in band 1 and molecular-like bosonic pairs in band 2. The total condensate is a coherent mixture of Cooper pairs and (almost) point-like molecular pairs.

(ii) for  $\Delta_2/E_{F_2} = 0.5$ , and also  $\omega_0/E_{F_2} = 2.5$ , the results are less extreme. We obtain  $k_{F_1}\xi_{\text{pair},1} = 10.6$  and  $k_{F_2}\xi_{\text{pair},2} = 2.2$ , with a ratio  $\Delta_2/\Delta_1 = 2.5$ . The Cooper pairs in band 2 start to overlap and the corresponding partial condensate is in the middle of the crossover regime between BCS and BEC (indeed in figure 8 the experimental point  $\Delta_2/E_{F_2} = 0.5$  is very close to the line  $\alpha = 0.5$  indicating the center of the crossover regime). This second case is very close to the experimental findings for the superconductor  $\text{Ba}_{0.6}\text{K}_{0.4}\text{Fe}_2\text{As}_2$  as reported in [14]. ( $\Delta_1 = 6$  meV,  $\Delta_2 = 12$  meV.)

We conclude with an observation concerning the results that we obtain by increasing the bottom band energy of the upper band. For  $\epsilon_2/E_{F_1} = 0.7$  (and same choice of  $\lambda_{11} = 0.15$ ,  $\lambda_{12} = \lambda_{21} = 0.05$ , 0.15 and 0.25) the BCS boundary line and the center of the crossover line for the partial condensate in the upper band ( $\alpha_2 = 0.2$  and 0.5 respectively) are almost not

affected by the different choice of  $\epsilon_2/E_{F_1}$ , as the corresponding values of the gap not much affected. On the other hand the boundary line  $\mu - \epsilon_2 = 0$  is placed to larger values of the coupling  $\lambda_{22}^{\text{eff}}$  and of the cutoff frequency  $\omega_0/E_{F_2}$ , and the corresponding gap  $\Delta_2/E_{F_2} \sim 7$  is also larger than in the case  $\epsilon_2/E_{F_1} = 0.5$ . One possible reason for this (unexpected) result is that the increased separation  $\epsilon_2$  between the bands leads to a larger density in band 1, determining a slower variation of the chemical potential  $\mu$  for increasing coupling.

## 4. Conclusions

We have analyzed the ground state superconducting properties of one- and two-band systems of fermions interacting through a separable attractive potential with an energy cutoff.

For the one-band system we have analyzed the behaviour of the superconducting gap, condensate fraction and pair correlation length as a function of coupling for different values of the cutoff. We have found that our model system gives expected results both in the weak- and in the strong-coupling limits. The pair correlation length and the superconducting gap recover the BCS limit for weak interactions, and the chemical potential approaches half of the binding energy of a bound state of two fermions in the BEC limit. By choosing three values for the condensate fraction we have defined the boundaries of the BCS, crossover and BEC regime of the BCS–BEC crossover, and we have determined the corresponding boundary values for the superconducting gap and for the pair correlation length. The superconducting gap to Fermi energy ratio is the most accessible physical quantity that can be measured in experiments. We have found that when the ratio between the gap and the Fermi energy is in the range  $0.55 < \Delta/E_F < 1.3$  the system is in the crossover regime of the BCS–BEC crossover for every value of the coupling and of the energy cutoff. Therefore this connection between  $\Delta/E_F$  and the crossover regime is not associated with the particular microscopic structure of the pairing interaction. The ratio  $\Delta/E_F$  results in a useful detection parameter to characterize the regime of the pairing of a superconductor, locating it in the BCS–BEC crossover.

For the two-band system we have analyzed the crossover boundary diagrams for the partial condensate fraction in the upper band and for the change of sign of the chemical potential relative to the bottom of the upper band. Different values of the interband coupling have been considered, assuming a weak-coupling regime of pairing in the lower band. We found that for increasing values of the interband coupling the access to the crossover regime is progressively anticipated with respect to the one-band case. The BEC regime for the partial condensate fraction is not reached in our range of coupling and energy cutoff because the presence of the lower band locks the chemical potential, retarding the change of sign of the chemical potential relative to the bottom of the upper band, and preventing the two-band system from accessing the BEC regime, thus widening the crossover regime of the BCS–BEC crossover.

In conclusion, our work gives a simple and quite general theoretical support to the recent ARPES measurements in iron-based superconductors which provide evidence that the Cooper pairs in the small Fermi surface form a condensate which is at the border between the crossover and the BEC regime. Therefore, the BCS–BEC crossover seems to be clearly realized in this new class of high- $T_c$  superconductors.

## Acknowledgments

We are grateful to A Bianconi, F Marsiglio, P Pieri and L Salasnich for useful discussions. We acknowledge financial support from the University of Camerino under the project FAR ‘Control and enhancement of superconductivity by engineering materials at the nanoscale’.

## References

- [1] Lin S Z and Hu X 2012 *New J. Phys.* **14** 063021
- [2] Leggett A J 1966 *Prog. Theor. Phys.* **36** 901
- [3] Marciani M, Fanfarillo L, Castellani C and Benfatto L 2013 *Phys. Rev. B* **88** 214508
- [4] Gillis S, Jyck J and Milošević M V 2014 *Phys. Rev. B* **89** 024512
- [5] Chaves A, Komendová L, Milošević M V, Andrade J S Jr., Farias G A and Peeters F M 2011 *Phys. Rev. B* **83** 214523
- [6] Komendová L, Chen Y, Shanenko A A, Milošević M V and Peeters F M 2012 *Phys. Rev. Lett.* **108** 207002
- [7] Lubashevsky Y, Lahoud E, Chashka E, Podolsky E and Kanigel A 2012 *Nat. Phys.* **8** 309
- [8] Gaebler J P, Stewart J P, Drake T E, Jin D, Perali A, Pieri P and Strinati G C 2010 *Nat. Phys.* **6** 569
- [9] Perali A, Palestini F, Pieri P, Strinati G C, Stewart J T, Gaebler J P, Drake T E and Jin D S 2011 *Phys. Rev. Lett.* **106** 060402
- [10] Shekhter A *et al* 2013 *Nature* **498** 75
- [11] Mishra V, Chatterjee U, Campuzano J C and Norman M R 2014 *Nat. Phys.* **10** 357
- [12] Perali A, Castellani C, di Castro C, Grilli M, Piegari E and Varlamov A A 2000 *Phys. Rev. B* **62** 9295
- [13] Perali A, Pieri P, Strinati G C and Castellani C 2002 *Phys. Rev. B* **66** 024510
- [14] Ding H *et al* 2008 *Europhys. Lett.* **83** 47001
- [15] Innocenti D, Poccia N, Ricci A, Valletta A, Caprara S, Perali A and Bianconi A 2010 *Phys. Rev. B* **82** 184528
- [16] Perali A, Bianconi A, Lanzara A and Saini N L 1996 *Solid State Commun.* **100** 181
- [17] Bianconi A 2005 *J. Supercond.* **18** 625
- [18] Perali A, Innocenti D, Valletta A and Bianconi A 2012 *Supercond. Sci. Technol.* **25** 124002
- [19] Shanenko A A, Croitoru M D, Zgirski M, Peeters F M and Arutyunov K 2006 *Phys. Rev. B* **74** 052502 and references therein
- [20] Borisenko S V *et al* 2012 *Symmetry* **4** 251
- [21] Bianconi A 2013 *Nat. Phys.* **9** 536
- [22] Mizohata Y, Ichioka M and Machida K 2013 *Phys. Rev. B* **87** 014505
- [23] Shanenko A A, Croitoru M D, Vagov A V, Axt V M, Perali A and Peeters F M 2012 *Phys. Rev. A* **86** 033612
- [24] Iskin M and Sá de Melo C A R 2006 *Phys. Rev. B* **74** 144517
- [25] Eagles D M 1969 *Phys. Rev.* **186** 456
- [26] Leggett A J 1980 *Modern Trends in the Theory of Condensed Matter (Lecture Notes in Physics)* ed A Pekalski and R Przystawa (Berlin: Springer) p 130
- [27] Salasnich L, Manini N and Parola A 2005 *Phys. Rev. A* **72** 023621
- [28] Pistolesi F and Strinati G C 1994 *Phys. Rev. B* **49** 6356
- [29] Suhl H, Matthias B T and Walker L R 1959 *Phys. Rev. Lett.* **3** 552
- [30] Marini M, Pistolesi F and Strinati G C 1998 *Eur. Phys. J. B* **1** 151
- [31] Schirotzek A, Shin Y, Schunck C H and Ketterle W 2008 *Phys. Rev. Lett.* **101** 140403
- [32] Okazaki K *et al* 2014 *Sci. Rep.* **4** 4109
- [33] Miao H *et al* 2014 arXiv:1406.0983